The new generation SLR station for time transfer with the sub-nanosecond accuracy and laser ranging with the sub-millimeter accuracy in the daytime and at night

M.A. Sadovnikov[1], *V.D. Shargorodskiy*[1] OJC «RPC «PSI», Moscow, Russia

Introduction

The modern tendencies of the satellite laser ranging development are determined by a few relevant tasks in the field of geodesy and navigation. In geodesy, it is creation of the globally integrated high-precision system of geodetic monitoring, the primary function of which is a comprehensive research of the Earth as the unified system by means of monitoring three basic components of the modern geodesy: geometrical shape and surface variations of the Earth, orientation and rotation parameters of the Earth and gravity field of the Earth [1].

The accomplishment of this task supposes the joint and coordinated use of data collected with the help of the basic instruments of space geodesy: SLR stations, VLBI interferometers, GNSS receivers, etc. Colocation of various instruments, i.e. installation of different-type devices on the same geographical spot and providing their mutual geodetic binding and their time scales synchronization, is of great importance.

In satellite navigation, a task of the navigation field precision increase at the expense of increasing precision of geodetic, ephemeris and frequency-time information, including data collected with the use of laser ranging, becomes more important [2]. Another particular task, although associated with the previous ones, is increasing precision of collation of the remote frequency and time standards for the purpose of increasing precision of the national and international time scales. The technology of laser time transfer can make a significant contribution to the accomplishment of this task [3]. In all the tasks listed above, the prospective SLR stations should provide the sub-millimeter accuracy on ranging and the accuracy on the level of a few tens of picoseconds on pseudoranging and time transfer, both in the daytime and at night. The prospective SLR stations should include GNSS receivers, measurements of which should be calibrated by laser measurements and then can be used for measurements correction of other, independently placed, reference or geodetic receivers.

Function, structure and technical characteristics of the new SLR station

The new SLR station is designed to perform high-precision measurements on geodetic and navigation spacecrafts with the purpose of:

- more precise definition of basic astronomic and geodetic parameters, PZ-90 reference frame parameters, parameters of connection between PZ-90 and ITRF;
- monitoring precision of geodetic, ephemeris and frequency-time parameters of ground-based and on-board segments of the GLONASS system;
- high-precision collation and synchronization of the GLONASS on-board and ground-based time scales with the time scale of the UTC (SU).

The new SLR station, the functional diagram of which is illustrated on Fig.1, includes 3 measuring systems: system of laser range measurements, system of laser pseudorange measurements and GNSS receiver.

The system of laser range measurements is a basic system that performs range tracking of the spacecrafts equipped with retroreflector systems, whose flight altitudes vary from 250 km to 25000 km, in the single-electron mode of return impulses receiving. The system of laser pseudorange measurements and time transfer performs high-precision measurements of laser impulses starting time in the time scale of the SLR station or external frequency-time standard. The pseudorange is determined taking into consideration the impulse on-board arrival time measurements performed by the on-board photodetector module, which is installed on the SC «Glonass». The divergence between the ground and on-board time scales that is

measured by the station and determined by the difference of laser range and pseudorange measurements is used for the time transfer.

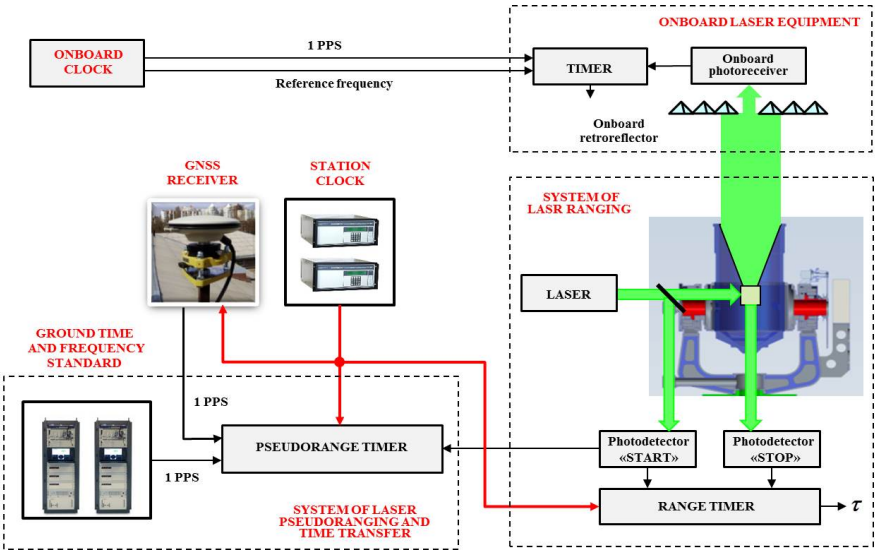

Fig. 1 Functional diagram of the new SLR station

The GNSS receiver measures the radiofrequency pseudorange by the code phase and by the carrier phase of the GNSS navigation signals. The receiver time scale is precisely synchronized with both station and external standard time scales, and its measurements are calibrated by laser pseudorange measurements. The basic technical characteristics of the new generation SLR station are given in Table 1.

Table 1

Parameter	Value
Receiving telescope main mirror diameter	360 mm
Telescope mount	AZ-EL
Transmitting telescope-refractor diameter	50 mm
Sensitivity of the star calibration camera (night/day)	14^m (4^m-6^m)
Daylight optical filter bandwidth	0.2 nm
Laser pulse energy	2.5 mJ
Laser pulse width	< 50 ps
Laser pulse repetition rate	1000 Hz
Laser beam divergence ($1/e^2$)	12” – 48”
Range measurement uncertainty (NP on the interval of 30 s)	< 1 mm
Pseudorange measurement uncertainty in its own and external time scales	< 25 ps

The problems of achieving the sub-millimeter accuracy of measurements

The creation of the laser station with the sub-millimeter accuracy level supposes reasonable improvement of random and systematic uncertainties of normal point (NP) formation by measurement results. The systematic uncertainties of NP formation appear in the bias of its value from the centroid of the single-electron distribution of the return impulses arrival. There are at least three physical effects causing the systematic bias $\Delta\tau_{NP}$ of the NP value.

First photon bias appears upon an increase of the average number of photoelectrons in return impulses n_{return} and consists in that the distribution of arrival times of photoelectrons shifts to the edge of a return impulse. The probability density of the distribution of the first photoelectron arrival times $p^1(t)$ normalized to the return impulse width depending on the average number of photoelectrons in the impulse n_{return} is illustrated on Fig. 2.

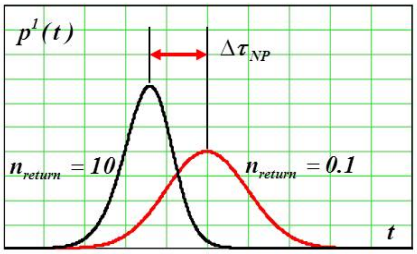

Fig. 2 Arrival times distribution for different values of the average number of photoelectrons

The bias value $\Delta\tau_{NP}$ is determined by the following formula:

$$\Delta\tau_{NP} = \frac{1}{2\sqrt{\pi}} \cdot n_{return} \cdot \sigma_{return}$$

where σ_{return} is the RMS width of a return impulse. If the average number of photoelectrons in an impulse is roughly equal to 1, the bias value of the distribution centroid for flat on-board retroreflector arrays reaches 20-80 ps.

Diffusion bias appears in the presence of an asymmetrical diffusion «tail» in the response function of the single-electron photodetector. When the iterative filtration of measurements with the use of the filtration window of a size $\mathbf{W=\pm n\cdot\sigma}$ (the value of n is usually selected in the range of 2…3) is applied, the centroid of the truncated distribution shifts to the distribution peak, as illustrated on Fig. 3.

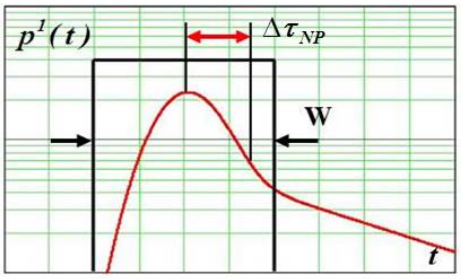

Fig. 3 Bias centroid of the distribution to its peak in the presence of the diffusion «tail» in the photodetector response and measurements screening in the $W=\pm n\sigma$ window

For photodetectors with the evident diffusion tail, the bias value can exceed 100 ps.

Background bias appears in the presence of measurements generated by the background photoelectrons. Large quantity of background measurements makes the centroid shift to the center of the filtration window, as illustrated on Fig. 4, increases the RMS deviation of the joint distribution of signal and background measurements and also increases the uncertainty of the centroid determination, even if the filtration window is centered relative to the centroid (because of the finite number of signal and background measurements).

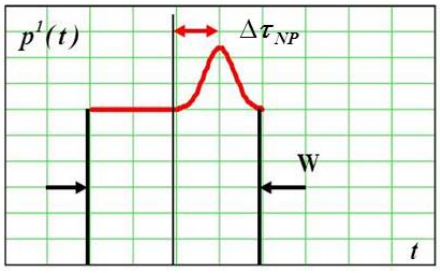

Fig. 4 Bias of the signal distribution centroid to the centroid of the joint signal and background measurements distribution

Differential method of laser ranging and normal point formation

To minimize the systematic uncertainties of NP formation, a differential method of measurements and normal point formation is applied in the laser station. The method lies in that the laser station simultaneously measures the times of the return pulse distribution both to a target and to the calibration retroreflector installed on the receiving telescope at the certain distance from the elevation axis of the pointing system. This method allows to:

- determine the laser station instrument correction by the calibration measurements directly at the moment of measurements taking;
- process the measurements in such a way that the systematic uncertainties are fully or partially compensated in the difference of range and calibration measurements.

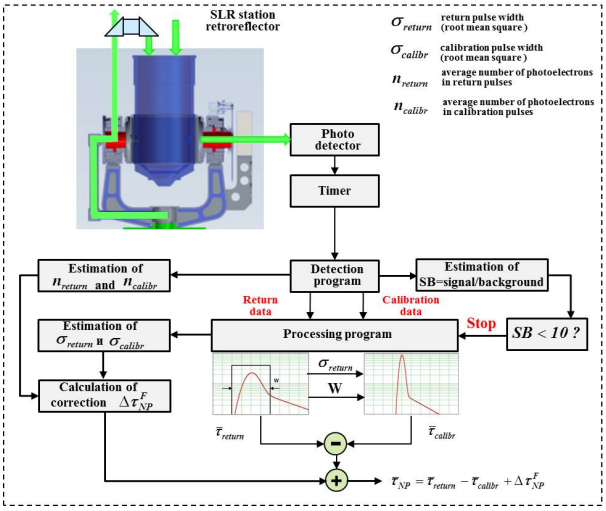

Fig. 5 Differential method of laser ranging and normal point formation

As illustrated on Fig. 5, when using this method, the detection program forms two arrays of measurement data: an array of range measurements and an array of calibration measurements. A normal point is generated by the processing program (a program of normal point generation) as a difference of the average values of range and calibration measurements.

To minimize the normal point diffusion bias, during the calculation of the average value by the array of calibration measurements the processing program uses the filtration window, the size of which is accorded to the iterative estimation of the RMS deviation σ_{return} by the array of range measurements and to the corresponding final size of the window $W = \pm n \cdot \sigma_{return}$ (basis of this method is given further).

To minimize the first photon bias, the detection program forms estimations of the average number of photoelectrons in the range and calibration impulses n_{return} and n_{calibr}. At the same time, with the purpose to minimize the background influence the processing program forms an estimation of the signal/background ratio (SB), i.e. an estimation of ratio of a number of measurements generated by return photoelectrons to a number of measurements generated by background photoelectrons.

Correction of the first photon bias is performed based on the following ratios [4]. On condition that there is no turbulent fluctuations of the atmosphere, the first photoelectron arrival times distribution is determined by the probability density of the following type:

$$p^1(t) = \lambda(t) \cdot exp\left[- \int_{-\infty}^{t} \lambda(t') \cdot dt' \right] \cdot \left[1 - exp(-n_{return}) \right]^{-1} \qquad (1)$$

where $\lambda(t)$ is the envelope of the return impulse. If the turbulent fluctuations of the atmosphere are strong, the probability density of the first photoelectron arrival is determined by the following formula:

$$p^{1b}(t_1, n_{se}) = \int_0^\infty p^1(t_1, n) \cdot \frac{1}{n_{return}} \cdot exp\left(\frac{n}{n_{return}}\right) \cdot dn \quad (2)$$

where t_1 is the first photoelectron arrival time normalized to the RMS width σ_{return} of the return impulse. Biases of the average time of photoelectron arrivals depending on the average number of photoelectrons in an impulse for cases when the turbulent fluctuations are and are not presented are determined by the following formulas:

$$\Delta\tau^1 = \sigma_{return} \cdot \int_{-\infty}^{\infty} t_1 \cdot p^1(t_1, n_{return}) \cdot dt_1 \text{ and } \Delta\tau^{1b} = \sigma_{return} \cdot \int_{-\infty}^{\infty} t_1 \cdot p^{1b}(t_1, n_{return}) \cdot dt_1$$

Calculations performed by these formulas show that the biases of the average time of photoelectron arrivals both in cases of the presence and absence of the fluctuations are almost equal and for $n_{return} \le 1$ are approximated by the following simple formula:

$$\Delta\tau = \frac{1}{2\sqrt{\pi}} \cdot n_{return} \cdot \sigma_{return}$$

In case of differential processing a normal point is formed as the difference between range and calibration measurements, so the final formula for the NP first photon bias correction has the appearance of:

$$\Delta\tau_{NP}^F = \frac{1}{2 \cdot \sqrt{\pi}} \cdot \left(n_{return} \cdot \sigma_{return} - n_{calibr} \cdot \sigma_{calibr}\right) \quad (3)$$

The NP bias caused by the presence of measurements generated by background photoelectrons can be estimated by the following formula:

$$\Delta\tau_{NP}^B = \frac{1 + SB}{SB} \cdot \sigma_{NP} \cdot \left(1 + \frac{n}{\sqrt{3 \cdot SB}}\right) \quad (4)$$

where SB is the signal/background ratio, σ_{NP} is the RMS deviation of a normal point on condition that there is no background, n is the coefficient that determines the size of the filtration window. It follows from the formula (4) that if the SB ratio is higher than 10, the indeterminacy of the NP value is increased by no more than 50%, that's why the detection program simply checks that $SB > 10$ is true, and if it is false, all the measurement data are considered inconsistent.

Method of the NP diffusion bias correction

The response functions (the probability densities of photoelectrons passing time distribution) of all single-electron photodetectors are asymmetrical and have a distinct diffusion «tail», the length of which is over several nanoseconds. The cause of the diffusion «tail» appearance can be explained by the fact, that a part of photoelectrons is generated outside the area of the strongly accelerating electric field, that is why such photoelectrons appear at the photodetector output with a delay.

During the filtration of measurements, the part of the diffusion «tail», not getting in the filtration window, is rejected, and that leads to the bias of the centroid of the response truncated function relative to the centroid of the initial response. The problem is that in fact the response function is the convolution of the photodetector's own response function and envelopes the pulse at its input. Range and calibration pulse's widths and shapes are not the same, that is why truncated range and calibration measurements biases are not the same either, and that causes the NP bias. The bias minimization can be reached by the reasonable selection of the photodetector and application of the differential method of NP formation, in which the calibration correction is not a constant value and one can select the size of the filtration window for the array of calibration measurements in such a way that the bias of the truncated range measurements will be compensated.

In the carried research the response function is determined by the four-parameter model, consisting of two components. The first component is the Gaussian kernel of the response function which depends on 2 parameters: the average passing time T_c and RMS deviation σ_c:

$$p_{core}(t,T_c,\sigma_c) = \frac{1}{\sqrt{2\pi}\cdot\sigma_c}\cdot exp\left(-\frac{(t-T_c)^2}{2\cdot\sigma_c^2}\right) \quad (5)$$

The second component of the response function is the diffusion component, which is determined by the convolution of the Gaussian kernel distribution with the exponential function that determines the diffusion delay in the photodetector; this function is defined by the parameter τ which is the diffusion tail decay time constant:

$$p_{tail}(t,T_c,\sigma_c,\tau) = \frac{1}{\sqrt{2\pi}\cdot\sigma_c}\cdot\int_{-\infty}^{\infty} exp\left(-\frac{(t-x-T_c)^2}{2\cdot\sigma_c^2}\right)\cdot\frac{1}{\tau}\cdot exp\left(-\frac{x}{\tau}\right)dx \quad (6)$$

The final response function $p_{pd}(t)$ is the weighted sum of the kernel and diffusion component with a parameter Δ which is equal to a portion of photoelectrons registered with the diffusion delay relative to the total number of the registered photoelectrons:

$$p_{pd}(t,T_c,\sigma_c,\tau,\Delta) = (1-\Delta)\cdot p_{core}(t,T_c,\sigma_c) + \Delta\cdot p_{tail}(t,T_c,\sigma_c,\tau) \quad (7)$$

Four parameters T_c, σ_c, τ and Δ are determined by the results of the analytical function (7) integration into the experimental response function, given in the photodetector's specification. Table 2 contains the approximating parameters, RMS deviations σ_{pd} and biases Δ_{bias} of the centroids in relation to the distributions peak for various types of the photodetectors: microchannel PM receiver MCP PMT R3809-74 with the resolution of 22 ps, hybrid photodetector Hybrid PD R10467U-40 with the resolution of 40 ps and photodetector SPAD K-14 with the resolution of 70 ps.

Table 2

Photodetector type	T_c	σ_c	τ	Δ	σ_{pd}	Δ_{bias}
MCP PMT R3809-74	1 ns	0.022 ns	0.25 ns	0.2	151 ps	50 ps
Hybrid PD R10467U-40	1 ns	0.04 ns	0.09 ns	0.2	67 ps	18 ps
SPAD K-14	1 ns	0.07 ns	0.4 ns	0.42	330 ps	168 ps

The approximated response functions of various types of the photodetectors (probability densities of the passing time distribution) are illustrated on Fig. 6, where the X-axis time is given in nanoseconds:

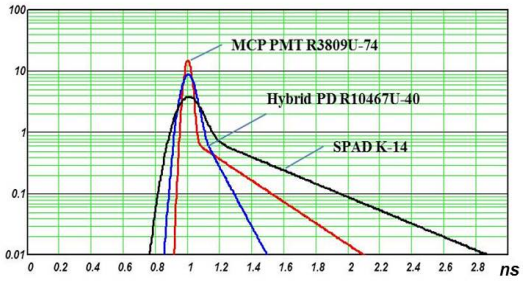

Fig. 6 Response functions for various types of the single-electron photodetectors

The response function centroid bias relative to the peak Δ_{bias} is the fundamental parameter of the photodetector that deserves a special definition (diffusion bias). This parameter gives the upper estimation of the uncertainty, introduced by the photodetector into the NP generation uncertainty. The RMS deviations of the response functions are equal to 151 ps for the microchannel PM receiver, 67 ps for the hybrid photodetector and 330 ps for the solid-

state photodetector. The values of the RMS deviations significantly exceed the resolution ratios of the photodetectors (the RMS deviations of response functions kernels). In the new generation SLR station, the calibration impulse width does not exceed 30 ps and the range impulse width may vary from 30 ps to 200 ps. In that case, the response functions become dependent on the impulse width and determined by the convolution of the Gaussian impulse at its input with the response function of the photodetector:

$$p_{data}(t,\sigma) = \frac{1}{\sqrt{2\pi}\cdot\sigma}\cdot\int_{-\infty}^{\infty} exp\left(-\frac{(t-x)^2}{2\cdot\sigma^2}\right)\cdot p_{pd}(x,T_c,\sigma_c,\tau,\Delta)\cdot dx \qquad (8)$$

Calculated by the formula (8), the response functions for range and calibration measurements are given on Fig. 7. For all the response functions, the centroid bias relative to the peak coincides with the diffusion biases of the photodetectors and is not dependent on the input impulse width. Because of that, the uncertainty of NP formation using the differential method is equal to 0, if at the stage of a normal point formation the non-truncated distributions of range and calibration measurements are used.

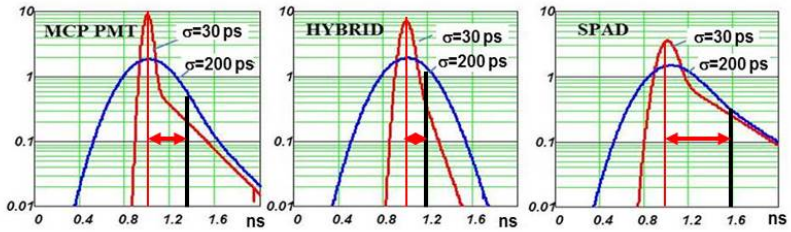

Fig. 7 Response functions for calibration and range measurements

From the other hand, if the input impulse width is equal to 200 ps, the RMS deviations of the response functions are equal to 250 ps for the microchannel PM receiver, 210 ps for the hybrid photodetector and 390 ps for the solid-state photodetector. To achieve the submillimeter accuracy of a normal point at these rates, it is required to perform more than 10000 measurements, that's why the truncation of the diffusion tails upon NP formation is mandatory. If the distributions are truncated, there appears the NP bias determined by the following ratio:

$$\Delta\tau_{NP}^{D} = m_{trunc}(\sigma_{return},n) - m_{trunc}(\sigma_{calibr},n) \qquad (9)$$

The mathematical expectations m_{trunk} (centroids) of the truncated distributions and their RMS deviations in the window of the size $\pm n\sigma$ can be calculated by the following formulas:

$$m_{trunc}(\sigma,n) = \sqrt{\left(\int_{1-n\sigma}^{1+n\sigma} t\cdot p_{trunc}(t,\sigma)\cdot dt\right)\cdot\left(\int_{1-n\sigma}^{1+n\sigma} p_{trunk}(t,\sigma)\cdot dt\right)^{-1}} - 1 \qquad (10)$$

$$\sigma_{trunc}(\sigma,n) = \sqrt{\left(\int_{1-n\sigma}^{1+n\sigma} (t-1)^2\cdot p_{trunc}(t,\sigma)\cdot dt\right)\cdot\left(\int_{1-n\sigma}^{1+n\sigma} p_{trunk}(t,\sigma)\cdot dt\right)^{-1}} \qquad (11)$$

in which the probability distribution density of the truncated data is equal to:

$$p_{trunc}(t,\sigma) = \left(p_{вых}(t,\sigma)\cdot\varphi(t)\right)\cdot\left(\int_{-\infty}^{\infty} p_{data}(t,\sigma)\,\varphi(t)\cdot dt\right)^{-1} \qquad (12)$$

where $\varphi(t)$ is a square function equal to 1 in the limits of the filtration window and to 0 beyond them. Table 3 shows the NP uncertainties calculated by the formulas (9-12) for cases when range and calibration measurements are filtrated in the separate windows, the sizes

of which are determined accordingly by the range and calibration impulses $\sigma_{return} = 200\ ps$ and $\sigma_{calibr} = 30\ ps$.

Table 3

Photodetector type	NP bias for n=3	NP bias for n=2
MCP PMT R3809-74	27 ps	16 ps
Hybrid PD R10467U-40	13 ps	9 ps
SPAD K-14	64 ps	34 ps

Table 4 presents the NP formation uncertainties calculated by the formulas (9-12) for cases when range and calibration measurements are filtrated in the same-size windows, the sizes of which are determined by the range impulse width σ_{return}.

Table 4

Photodetector type	NP bias for n=2.5		
	$\sigma_{return} = 200\ ps$	$\sigma_{return} = 100\ ps$	$\sigma_{return} = 50\ ps$
MCP PMT R3809-74	-4.1 ps	-1.1 ps	-0.1 ps
Hybrid PD R10467U-40	-2.3 ps	-0.9 ps	-0.02 ps
SPAD K-14	3.5 ps	2.8 ps	0.7 ps

Thus, in range and calibration data filtration in the separate windows of the optimal sizes the NP value bias may considerably exceed the millimeter level of the accuracy of measurements. In case of the data filtration in the same-size windows, the NP value bias is on the sub-millimeter level.

Conclusion

The new generation SLR station incorporates laser and radio measurement means and is designed to perform geodetic, time transfer and GLONASS ephemeris and time support accuracy increase tasks. To achieve the sub-millimeter accuracy of range measurements, the single-electron receiving mode and differential method of laser ranging and normal point formation are used in the laser station. Because of its minimal value of the diffusion bias, the hybrid single-electron photodetector is selected for use in the SLR station.

References

[1] Plag H., Pearlman M., The Global Geodetic Observing System: meeting the requirements of a global society on changing planet in 2020 // Springer Verlag 2009.

[2] Baryshnikov M.V., Sadovnikov M.A., Shargorodskiy V.D., The concept of the use of satellite laser ranging for improvement of GLONASS accuracy // Mir izmereniy, № 8, 2014.

[3] Baryshnikov M.V., Sadovnikov M.A., Shargorodskiy V.D., Comparison and transfer of time scale with a subnanosecond accuracy on laser measurements of range and pseudorange // VII International symposium “Metrology of time and space”, Suzdal, Russia, 2014.

[4] Sadovnikov M.A., Pulse repetition rate optimization in SLR stations to provide minimum systematic error of ranging // Proceedings of the 16th International workshop on laser ranging, Poznan, Poland, 2008.